Eur. Phys. J. B **13**, 765–775 (2000)

THE EUROPEAN PHYSICAL JOURNAL B

EDP Sciences

Heteroclinic behavior in rotating Rayleigh-Bénard convection

A. Demircan, S. Scheel[a], and N. Seehafer[b]

Institut für Physik, Universität Potsdam, PF 601553, 14415 Potsdam, Germany

Received 10 June 1999

Abstract. We investigate numerically the appearance of heteroclinic behavior in a three-dimensional, buoyancy-driven fluid layer with stress-free top and bottom boundaries, a square horizontal periodicity with a small aspect ratio, and rotation at low to moderate rates about a vertical axis. The Prandtl number is 6.8. If the rotation is not too slow, the skewed-varicose instability leads from stationary rolls to a stationary mixed-mode solution, which in turn loses stability to a heteroclinic cycle formed by unstable roll states and connections between them. The unstable eigenvectors of these roll states are also of the skewed-varicose or mixed-mode type and in some parameter regions skewed-varicose like shearing oscillations as well as square patterns are involved in the cycle. Always present weak noise leads to irregular horizontal translations of the convection pattern and makes the dynamics chaotic, which is verified by calculating Lyapunov exponents. In the nonrotating case, the primary rolls lose, depending on the aspect ratio, stability to traveling waves or a stationary square pattern. We also study the symmetries of the solutions at the intermittent fixed points in the heteroclinic cycle.

PACS. 47.20.Ky Nonlinearity (including bifurcation theory) – 47.20.Bp Buoyancy-driven instability – 47.32.-y Rotational flow and vorticity – 47.54.+r Pattern selection; pattern formation

1 introduction

Rayleigh-Bénard convection in a plane fluid layer heated from below and rotating about a vertical axis has been an object of special interest due to its geophysical and astrophysical applications, its realizability in laboratory experiments, and since it allows a theoretical study of pattern formation and the transition to turbulence. For a plane fluid layer of infinite horizontal extent, with stress-free top and bottom boundaries, as well with infinite Prandtl number, Küppers and Lortz [1] found two-dimensional, stationary convection rolls to be unstable if the Taylor number, measuring the rotation rate, exceeds the critical value $T_c = 2\,285$. This result was obtained by using a small-amplitude expansion near the onset of convection. The instability, known as the Küppers-Lortz instability, appears in the form of rolls rotated by about 58° with respect to the original rolls, and the new, rotated rolls are in turn unstable to rolls rotated relative to them.

Küppers [2], Clever and Busse [3], and Clune and Knobloch [4] extended the analysis to the case of rigid boundaries and finite Prandtl number, where the instability also occurs. It was found that the critical Taylor number above which no stable two-dimensional rolls exist decreases with decreasing Prandtl number. For Taylor numbers below the critical one the situation is complicated by the fact that the instability mechanisms for rolls in a nonrotating system (see, *e.g.*, Busse and Clever [5] or Busse [6]) continue to operate and compete with the Küppers-Lortz mechanism. In particular, the Küppers-Lortz instability is closely related to the skewed-varicose instability, and the two instabilities cannot always be distinguished. For fixed values of the Prandtl number and the Taylor number, there exist stability regions for rolls in the plane of the (basic) wave number (measuring the diameter of the rolls) and the Rayleigh number [3]. Roughly, the rolls exist in finite Rayleigh-number intervals near the onset of convection and become skewed-varicose or Küppers-Lortz unstable if the Rayleigh number exceeds threshold values depending on wave number, Prandtl number and Taylor number. The angle χ between the most unstable Küppers-Lortz perturbation and the unperturbed rolls is also parameter-dependent, but for high rotation rates and large Prandtl numbers the values of χ lie in the neighborhood of 58°, the angle found by Küppers and Lortz [1] for the case of free-slip boundary conditions. For these latter conditions there exists still another, small-angle instability which, unlike the familiar Küppers-Lortz instability, disappears at infinite Prandtl number and does not occur for no-slip boundary conditions (see Ref. [4] and the recent study by Ponty, Passot, and Sulem [7]).

When stationary rolls have become unstable through the Küppers-Lortz instability, the convection is inevitably time-dependent. Busse, Clever, and Heikes [8,9] modeled

[a] *Present address*: Theoretisch-Physikalisches Institut, Friedrich-Schiller-Universität Jena, Max-Wien-Platz 1, 07743 Jena, Germany

[b] e-mail: `seehafer@agnld.uni-potsdam.de`

the resulting dynamical behavior by a system of three ordinary differential equations describing the interaction between just three relevant Fourier modes. These modes correspond to rolls which are transformed into each other by 60^o rotations. The three roll states are cyclically visited by the system. This was found numerically [8,9], but the existence and stability (time-asymptotic as well as structural) of a heteroclinic cycle for the three-dimensional model has also been proved mathematically [10–12]. Goldstein, Knobloch, and Silber [13] used equivariant (symmetric) bifurcation theory to study the onset of convection for the case of horizontal periodicity on a hexagonal lattice. Assuming the unstable disturbances to be nonoscillatory (oscillatory onset of convection is only possible for Prandtl numbers less than 0.677 [14], this upper bound applying to free-slip as well as no-slip boundary conditions [4]), they derived a system of three characteristic ordinary differential equations, valid close to the onset of convection and containing the model system of Busse, Clever, and Heikes [8,9] as a truncated version. It was found that for appropriate values of the system parameters, as the essence of the Küppers-Lortz instability, heteroclinic orbits connecting roll solutions appear.

Heteroclinic behavior was also observed in theoretical studies of nonrotating convection. As found by Busse and Bolton [15,16], in the case of stress-free top and bottom boundaries stable convection rolls cannot exist for Prandtl numbers less than about 0.5 and convection rolls with the critical wave number (for the onset of convection) are always unstable. Like rotation, this provides possibilities for a direct transition from the quiescent basic state to complicated spatiotemporal behavior. Heteroclinic behavior in nonrotating convection at low Prandtl numbers and between stress-free top and bottom boundaries was observed in numerical bifurcation studies by Busse, Kropp, and Zaks [17] and Matthews *et al.* [18]. These authors used aspect (*i.e.*, width to depth) ratios of 8 (Ref. [17]) and 1, respectively, and obtained parts of their results by studying low-order systems of model equations.

Heteroclinic orbits give rise to a nonstationary, intermittent dynamics similar to what is observed in many experiments. If the attracting state is a stable heteroclinic cycle, on the other hand, the intermittent behavior disappears as time evolves since the system comes closer and closer to the unstable fixed points and spends more and more time in their vicinity. For this reason Busse, Clever, and Heikes [8,9] introduced noise into their model, numerically realized by lower bounds for the moduli of the three dynamical variables. If these lower bounds fluctuate randomly, the temporal behavior is expected to be statistically periodic and at the same time irregular.

In recent years both experimental [19–21] and numerical [22] studies of rotating convection have predominantly been concentrated on systems with large aspect ratios (aspect ratios larger than about 10). Spatially extended convective systems appear particularly suitable for the study of structure formation and (the transition to) spatiotemporal chaos [23–25]. While in reference [22] the original hydrodynamic equations (in the Boussinesq approximation) are solved, other theoretical investigations of the subject use model equations, notably of the Swift-Hohenberg type [26–29]. Recent numerical studies of rapidly rotating turbulent convection in a plane periodic geometry with small aspect ratio are due to Julien *et al.* [30,31].

The numerical studies of convective systems on the base of the original hydrodynamic equations use mainly simulations of the equations, forward in time and starting from selected or random initial conditions. By providing information on the time-asymptotic states for given values of the system parameters, simulations are a valuable tool to determine the bifurcation structure of the systems studied. In general, systems with small aspect ratios are more accessible to bifurcation analyses than such with large aspect ratios. One obvious reason is that the required high number of grid or collocation points limits the numerical analysis of large systems. Due to restricted computer capacities, specific numerical methods of bifurcation analysis [32] are presently, if at all, only applicable to small-aspect-ratio systems. Furthermore, the experimental observations indicate qualitative differences between small-scale and large-scale systems in that for the latter ones the transition to time dependence, complexity and chaos does not seem to be characterized by a sequence of well separable and mainly supercritical bifurcations and is thus difficult to analyze. But also for the seemingly simpler small-scale systems the transition to time dependence and chaos is still imperfectly understood.

There exist important applications where the aspect ratio is small or moderate. The fluid outer core of the Earth is a spherical shell whose thickness is approximately equal to the mean value of the inner and outer radii, giving an "azimuthal aspect ratio" of about three and an "axial aspect ratio" of about one (needless to say, the spherical-shell topology is important here; plane geometry with periodic horizontal boundary conditions as assumed in many theoretical studies reflects at least the azimuthal periodicity of the spherical geometry). The corresponding aspect ratios for the convection zone of the Sun (also a spherical shell) are 9 and 2, respectively. Also a number of methods for semiconductor crystal growth from a crystal melt, in particular those where the melt is situated in a (rotating) vertical heated crucible, correspond to convection with a small aspect ratio and allow at least important aspects to be modeled by Rayleigh-Bénard configurations with heating from below and cooling from above [33].

Recent laboratory experiments on rotating convection with water in containers with aspect ratio ≈ 1 are reported in references [34,35] for a circular convection cell and in reference [36] for a rectangular convection cell. A particular property of rotating convection in small-aspect-ratio circular containers is a lowering of the critical Rayleigh number for the convection onset compared to the predictions for a laterally infinite system [14]. This is caused by special non-axisymmetric modes which are spatially localized near the lateral boundary and which show an azimuthal pattern drift. References [37,38] describe experiments with water in circular containers, with radius to depth ratio 2.5 and 5, respectively, and concentrate

particularly on the observation of these sidewall traveling waves and their description by the complex Ginzburg-Landau equation. Using the basic hydrodynamic equations, Goldstein *et al.* [39] have numerically solved the linear stability problem for the onset of convection in the rotating cylinder. They found that there is a competition between sidewall modes and bulk or body modes and that sidewall modes set in first if the aspect ratio is sufficiently small. A remarkable experimental observation was made by Bajaj *et al.* [40]: For water in a circular container with radius to depth ratio $\Gamma = 4.8$ as well for argon in a container with $\Gamma = 8.3$, and for rotation rates where Küppers-Lortz dynamics is theoretically expected, they found square patterns near the onset of convection (by onset the appearance of bulk modes is meant here; in addition the wall mode can be present along the cell periphery). Other experiments on rotating convection, including early work, are discussed in the monograph of Koschmieder [41], who stresses the role of centrifugal effects.

In this paper we consider a rotating system with small aspect ratio and concentrate on the appearance and properties of heteroclinic behavior for small to moderate rotation rates. We use periodic boundary conditions in the horizontal directions. Clearly, special sidewall effects, like the wall modes in circular geometry, are filtered out by these boundary conditions. The influence of walls at a finite distance appears through the finite aspect ratio. A general study would require a variation of the aspect ratio, in addition to and independent of variations of the Rayleigh, Taylor, and Prandtl numbers. This is an unrealistic undertaking for a single numerical study. Therefore the aspect ratio is kept fixed at a value of $2\sqrt{2}$ in most of the calculations and at values of 4, 4.5, or $4\sqrt{2}$ in a few additional calculations. The Prandtl number is 6.8. By these parameter choices the present study continues recent investigations of two-dimensional [42] and three-dimensional [43] nonrotating convection with the same parameters. In rotating convection the horizontal length scale decreases with increasing rotation rate, which corresponds to an increase of the effective aspect ratio. By varying the rotation rate we thus scan, to a certain degree, also the aspect ratio. This method to vary the effective aspect ratio has been exploited in experiments [36,37]. At the top and bottom stress-free boundary conditions are used, which are appropriate for many geophysical and astrophysical applications and are computationally simpler than no-slip conditions. The system is supposed to rotate about the vertical z axis. This can be viewed as looking at the polar region of a star or planet. As in all of the above mentioned theoretical studies of rotating convection, it is assumed that the centrifugal force is negligible in comparison with gravity, so that the effects of rotation appear through the Coriolis force only. For our small aspect ratios and relatively low rotation rates the neglect of the centrifugal force is unproblematic. As to the applicability of our results to systems with large aspect ratios it should be noted that the physical mechanisms observed in small-scale systems can act locally in large-scale systems too.

After introducing the governing equations in Section 2, we describe two-dimensional convection rolls and their symmetries under the influence of rotation in Section 3. The appearance and properties of heteroclinic behavior are studied in Sections 4 and 5. In Section 6 a discussion of our results is given.

2 Equations

We consider buoyancy-driven rotating convection in a plane fluid layer of thickness d heated from below. Using the Oberbeck-Boussinesq approximation, the governing system of partial differential equations reads as follows:

$$\frac{\partial \mathbf{v}}{\partial t} + (\mathbf{v}\cdot\nabla)\mathbf{v} = -\nabla p + \mathcal{P}\triangle\mathbf{v} + \mathcal{P}\mathcal{R}\,\theta\mathbf{e}_z + \mathcal{P}\sqrt{\mathcal{T}}\,\mathbf{v}\times\mathbf{e} \tag{1}$$

$$\nabla\cdot\mathbf{v} = 0 \tag{2}$$

$$\frac{\partial \theta}{\partial t} + \mathbf{v}\cdot\nabla\theta = v_z + \triangle\theta\,. \tag{3}$$

Here $\mathbf{v}$ is the fluid velocity and p and θ represent the deviations of pressure and temperature from their values in the pure conduction state. We use Cartesian coordinates x, y and z with the z axis in the vertical direction parallel to the gravitational force. $\mathbf{e}_z$ is the unit vector in the vertical direction whereas the vector $\mathbf{e}$ is the general notation for the unit vector in the direction of the rotation axis. For our special choice $\mathbf{e} = \mathbf{e}_z$ one has $\mathbf{v}\times\mathbf{e} = (v_y, -v_x, 0)$ in equation (1). Equations (1–3) are given in dimensionless form where the units of length and time are d and d^2/κ, respectively, with κ being the thermal diffusivity. θ is measured in units of the temperature difference δT between the lower and upper boundaries of the fluid layer. There are three dimensionless parameters, the Prandtl number $\mathcal{P}$, the Rayleigh number $\mathcal{R}$, and the Taylor number $\mathcal{T}$, defined by

$$\mathcal{P} = \frac{\nu}{\kappa}, \qquad \mathcal{R} = \frac{\alpha g d^3}{\nu\kappa}\delta T, \qquad \mathcal{T} = \left(\frac{2\Omega d^2}{\nu}\right)^2, \tag{4}$$

where ν is the kinematic viscosity, α the volumetric expansion coefficient, Ω the angular velocity of the rotation and g the gravitational acceleration. The Rayleigh number $\mathcal{R}$ measures the strength of the buoyancy forces.

We apply periodic boundary conditions with spatial period L in the horizontal directions x and y. The top and bottom planes are assumed to be impenetrable, stress-free and isothermal:

$$\frac{\partial v_x}{\partial z} = \frac{\partial v_y}{\partial z} = v_z = \theta = 0 \quad \text{at } z = 0, 1. \tag{5}$$

For the choice of boundary conditions the following Fourier expansions are appropriate:

$$v_x = \sum_{k_x,k_y=-\infty}^{\infty}\sum_{k_z=0}^{\infty} \tilde{v}_x(\mathbf{k})\mathrm{e}^{\mathrm{i}k_x x + \mathrm{i}k_y y}\cos k_z z \tag{6}$$

$$v_y = \sum_{k_x,k_y=-\infty}^{\infty} \sum_{k_z=0}^{\infty} \tilde{v}_y(\mathbf{k}) \mathrm{e}^{\mathrm{i}k_x x + \mathrm{i}k_y y} \cos k_z z \qquad (7)$$

$$v_z = \sum_{k_x,k_y=-\infty}^{\infty} \sum_{k_z=0}^{\infty} \tilde{v}_z(\mathbf{k}) \mathrm{e}^{\mathrm{i}k_x x + \mathrm{i}k_y y} \sin k_z z \qquad (8)$$

$$\theta = \sum_{k_x,k_y=-\infty}^{\infty} \sum_{k_z=0}^{\infty} \tilde{\theta}(\mathbf{k}) \mathrm{e}^{\mathrm{i}k_x x + \mathrm{i}k_y y} \sin k_z z \qquad (9)$$

$$p = \sum_{k_x,k_y=-\infty}^{\infty} \sum_{k_z=0}^{\infty} \tilde{p}(\mathbf{k}) \mathrm{e}^{\mathrm{i}k_x x + \mathrm{i}k_y y} \cos k_z z. \qquad (10)$$

The wave numbers $\mathbf{k} = (k_x, k_y, k_z)$ are connected with the integer mode numbers $\mathbf{n} = (n_x, n_y, n_z)$ by

$$k_x = n_x \frac{2\pi}{L}, \qquad n_x = 0, \mp 1, \mp 2, \ldots \qquad (11)$$

$$k_y = n_y \frac{2\pi}{L}, \qquad n_y = 0, \mp 1, \mp 2, \ldots \qquad (12)$$

$$k_z = n_z \pi, \qquad n_z = 0, 1, 2, 3, \ldots \qquad (13)$$

With the abbreviations

$$\mathbf{w} = (\mathbf{v} \cdot \nabla)\mathbf{v}\,, \qquad \phi = \mathbf{v} \cdot \nabla\theta \qquad (14)$$

for the nonlinearities, which have Fourier expansions like $\mathbf{v}$ and θ, we arrive at the analogues of equations (1–3) in Fourier space:

$$0 = \mathrm{i}k_x \tilde{v}_x + \mathrm{i}k_y \tilde{v}_y + k_z \tilde{v}_z \qquad (15)$$

$$\dot{\tilde{v}}_x = -\mathrm{i}k_x \tilde{p} - \tilde{w}_x - \mathcal{P}\,\mathbf{k}^2 \tilde{v}_x + \mathcal{P}\sqrt{\mathcal{T}}\,\tilde{v}_y \qquad (16)$$

$$\dot{\tilde{v}}_y = -\mathrm{i}k_y \tilde{p} - \tilde{w}_y - \mathcal{P}\,\mathbf{k}^2 \tilde{v}_y - \mathcal{P}\sqrt{\mathcal{T}}\,\tilde{v}_x \qquad (17)$$

$$\dot{\tilde{v}}_z = k_z \tilde{p} - \tilde{w}_z - \mathcal{P}\,\mathbf{k}^2 \tilde{v}_z + \mathcal{P}\mathcal{R}\,\tilde{\theta} \qquad (18)$$

$$\dot{\tilde{\theta}} = \tilde{v}_z - \tilde{\phi} - \mathbf{k}^2 \tilde{\theta}. \qquad (19)$$

Due to the constraint (2) not all of these equations are independent of each other. By taking the divergence of equation (1) one eliminates the pressure p, namely,

$$\tilde{p} = \mathrm{i}\frac{k_x}{\mathbf{k}^2}\left(\tilde{w}_x - \mathcal{P}\sqrt{\mathcal{T}}\,\tilde{v}_y\right) + \mathrm{i}\frac{k_y}{\mathbf{k}^2}\left(\tilde{w}_y + \mathcal{P}\sqrt{\mathcal{T}}\,\tilde{v}_x\right) + \frac{k_z}{\mathbf{k}^2}\left(\tilde{w}_z - \mathcal{P}\mathcal{R}\,\tilde{\theta}\right). \qquad (20)$$

Equations (16, 17) can now be written as

$$\dot{\tilde{v}}_x = \left(\frac{k_x^2}{\mathbf{k}^2} - 1\right)\left(\tilde{w}_x - \mathcal{P}\sqrt{\mathcal{T}}\,\tilde{v}_y\right) - \mathcal{P}\mathbf{k}^2\tilde{v}_x + \frac{k_x k_y}{\mathbf{k}^2}\left(\tilde{w}_y + \mathcal{P}\sqrt{\mathcal{T}}\,\tilde{v}_x\right) + \mathrm{i}\frac{k_x k_z}{\mathbf{k}^2}\left(\mathcal{P}\mathcal{R}\tilde{\theta} - \tilde{w}_z\right) \qquad (21)$$

$$\dot{\tilde{v}}_y = \left(\frac{k_y^2}{\mathbf{k}^2} - 1\right)\left(\tilde{w}_y + \mathcal{P}\sqrt{\mathcal{T}}\,\tilde{v}_x\right) - \mathcal{P}\mathbf{k}^2\tilde{v}_y + \frac{k_x k_y}{\mathbf{k}^2}\left(\tilde{w}_x - \mathcal{P}\sqrt{\mathcal{T}}\,\tilde{v}_y\right) + \mathrm{i}\frac{k_y k_z}{\mathbf{k}^2}\left(\mathcal{P}\mathcal{R}\tilde{\theta} - \tilde{w}_z\right). \qquad (22)$$

As in [43] we restrict ourselves to the case of a vanishing mean horizontal flow since such flows can be removed by a Galilean transformation. Therefore we set $\tilde{v}_x(0,0,0) = \tilde{v}_y(0,0,0) = 0$.

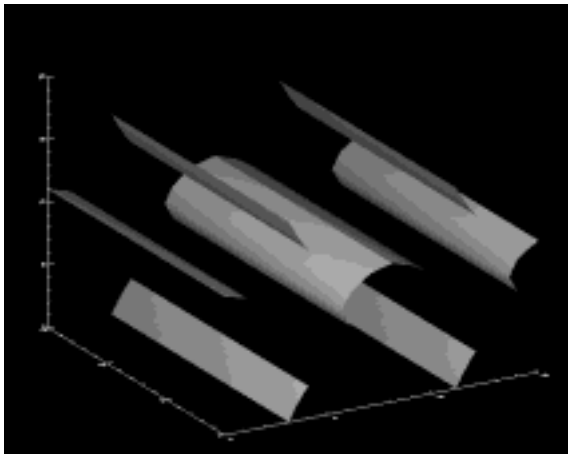

Fig. 1. Convection rolls at $\mathcal{R} = 10\,000$ without rotation.

3 Two-dimensional stable rolls under the influence of rotation

In our numerics we used a pseudospectral method [44,45] with in general 16 collocation points in each spatial direction; to test for truncation (or finite-resolution) effects, additional calculations were made with a resolution of 32 collocation points in each of the horizontal directions (and 16 points in the vertical direction). Time integration was performed using an eighth-order Runge-Kutta scheme as described in [46]. Starting from a nonrotating stationary state with two-dimensional straight convection rolls [43], depicted in Figure 1, we performed calculations with increasing Taylor number $\mathcal{T}$. As is well-known, the convection rolls remain stable as long as the rotation is sufficiently slow.

The periodic horizontal boundary conditions restrict the possible angles α between the rolls and (say) the y axis under which parallel rolls can be put in a periodic box. For a general rectangular periodicity box one finds

$$\begin{aligned} 2nD/\cos\alpha &= L_x, \\ 2mD/\sin\alpha &= L_y, \end{aligned} \qquad (23)$$

where L_x and L_y are the side lengths of the box, D is the roll diameter, and m and n are integer numbers. The periodic boundary conditions require that even numbers of rolls cross the sides of the rectangle. Relations (23) give the necessary and sufficient condition

$$mL_x \cos\alpha = nL_y \sin\alpha. \qquad (24)$$

In our special case of a quadratic box this condition takes the form

$$m\cos\alpha = n\sin\alpha \qquad (25)$$

and the roll diameter is

$$D = \frac{L}{2n}\cos\alpha = \frac{L}{2m}\sin\alpha. \qquad (26)$$

The choice $m = n = 1$, for instance, implies $\alpha = 45^{\circ}$ or $\alpha = 225^{\circ}$, respectively. The roll states observed are invariant with respect to rotations by 180° about the vertical (see below); thus $\alpha = 45^{\circ}$ and $\alpha = 225^{\circ}$ correspond to the same state. For $m = 1$ and $n = -1$ one finds $\alpha = -45^{\circ}$, $m = 1$ and $n = 2$ give $\alpha = 26.6^{\circ}$, and so on. In Fourier space the states with nonrotated or rotated straight rolls are easily detected since only modes with horizontal wave vectors (k_x, k_y) perpendicular to the roll axis are excited. So for rolls rotated by 45° with respect to the original orientation parallel to the y axis only modes with $k_x = k_y$ and for rolls rotated by -45° only modes with $k_x = -k_y$ are present.

For not too high Rayleigh numbers, the convection for $\mathcal{T} = 0$ (no rotation) is purely two-dimensional and time-independent, in the form of rolls parallel to the y axis (parallel to one of the sides of the square box). In [43] we found the formal structure of the symmetry group $\mathcal{G}$ under which the steady-state solution is invariant to be $[D_2]_{x,z} \times O(2)_y \times SO(2)_t$. Under the influence of (slow) rotation the rolls are still present, still parallel to one of the sides of the square, and still stationary. Unlike in the nonrotational case, also the velocity component v_y has non-zero values; under the influence of the Coriolis force the velocity streamlines are no longer perpendicular to the roll axis. The Fourier modes of all field components are still y-independent, *i.e.*, all modes with mode numbers (i, j, k), $j \neq 0$ vanish.

Inspection of the Fourier coefficients of the state of a slowly rotating system shows that the following symmetry relations still hold:

$$\tilde{v}_x(i,j,k) = \tilde{v}_y(i,j,k) = \tilde{v}_z(i,j,k) = \tilde{\theta}(i,j,k) = 0 \qquad i + k \text{ odd}. \quad (27)$$

It has been noted in [43] that the corresponding symmetry operation $T_{\mathrm{ud}}^{L/2}$ (called S_2 in Ref. [43]) is an up-down reflection (a reflection in the x-y plane or horizontal midplane) combined with a translation of the pattern in the x direction by $L/2$:

$$T_{\mathrm{ud}}^{L/2}: \quad (x,y,z) \mapsto (x + \frac{L}{2}, y, 1-z)$$
$$(v_x, v_y, v_z, \theta) \mapsto (v_x, v_y, -v_z, -\theta). \quad (28)$$

Furthermore one finds that (provided $x = 0$ is just the midplane between two neighboring, counterrotating rolls)

$$\begin{aligned} \tilde{v}_x(i,j,k) &= -\tilde{v}_x(-i,-j,k) \\ \tilde{v}_y(i,j,k) &= -\tilde{v}_y(-i,-j,k) \\ \tilde{v}_z(i,j,k) &= \tilde{v}_z(-i,-j,k) \\ \tilde{\theta}(i,j,k) &= \tilde{\theta}(-i,-j,k), \end{aligned} \quad (29)$$

which corresponds to symmetry with respect to rotations T_{180} by 180° about the vertical (called S_6 in Ref. [43]):

$$T_{180}: \quad (x,y,z) \mapsto (-x,-y,z)$$
$$(v_x, v_y, v_z, \theta) \mapsto (-v_x, -v_y, v_z, \theta). \quad (30)$$

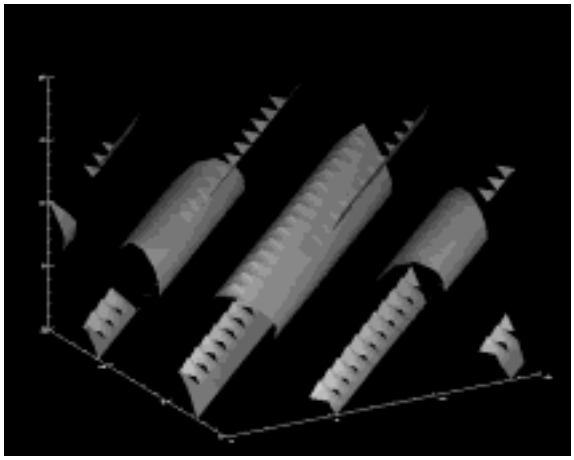

Fig. 2. One of the intermittent fixed points at $\mathcal{R} = 10\,000$ and $\mathcal{T} = 400$.

The transformations $T_{\mathrm{ud}}^{L/2}$ and T_{180} generate the discrete group $\mathcal{G}_d = \{T_{\mathrm{ud}}^{L/2}, T_{180}, T_{\mathrm{ud}}^{L/2} T_{180}, \mathrm{id}\}$. $\mathcal{G}_d$ has the group structure D_2, that is, it is commutative, each element is inverse to itself, and the product of two different nontrivial elements (*i.e.*, elements that are different from the identical transformation id) gives the third nontrivial element. Together with the translational invariance and the periodicity in the y direction (along the roll axis), which correspond to a circular symmetry $SO(2)$, the formal structure of the symmetry group of the roll states is then $[D_2]_{x,y,z} \times SO(2)_y \times SO(2)_t$. Compared to the nonrotating case one reflection symmetry is lost. This results from the fact that the Coriolis force breaks reflection symmetry in vertical planes.

4 Transition to heteroclinic behavior for fixed Rayleigh number

For $\mathcal{R}$ fixed at a value of 10 000, our numerical calculations show a transition from stationary roll convection to heteroclinic behavior at a Taylor number of $\mathcal{T} = 360$. Typical three-dimensional surface plots of the modulus of the velocity field are shown in Figures 2 and 3. The temporal evolution of the absolute values of the modes $\tilde{v}_x(-1,1,1)$ and $\tilde{v}_x(1,1,1)$ is depicted in Figure 4. The intermittent, unstable fixed points correspond to rolls rotated by either -45° or $+45^{\circ}$ with respect to the original rolls parallel to the y axis. So it is seen in Figure 4 that always either the mode $(-1,1,1)$ (which corresponds to rolls rotated by -45°) or the mode $(1,1,1)$ (which corresponds to rolls rotated by $+45^{\circ}$) is excited.

The unstable, rotated rolls are still straight and still invariant under the symmetry group of the stable rolls (described in Sect. 3). This is easily checked by means of the conditions (27, 29) (in the case of condition (29) one has to ensure that the planes $x = -y$ or $x = y$, respectively, are midplanes between neighboring, counterrotating rolls).

The temporal behavior shown in Figure 4 was obtained after a long simulation. The time the system spends

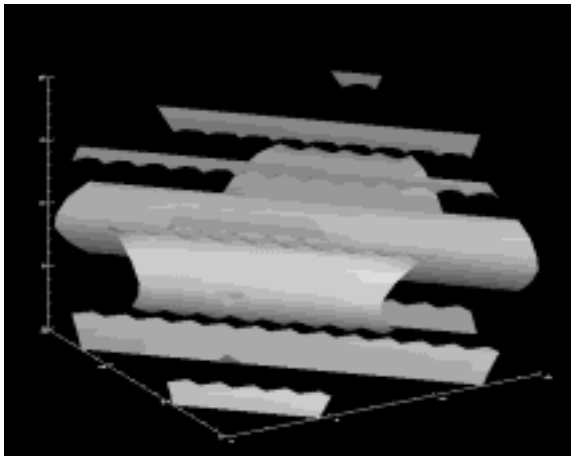

Fig. 3. Another intermittent fixed point at $\mathcal{R} = 10\,000$ and $\mathcal{T} = 400$.

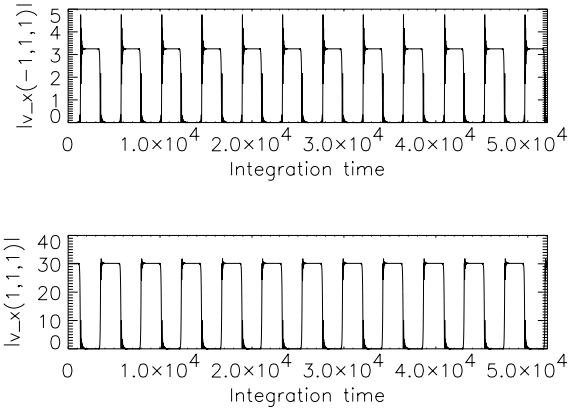

Fig. 4. Time evolution of the absolute values of the modes $\tilde{v}_x(-1,1,1)$ and $\tilde{v}_x(1,1,1)$ at $\mathcal{R} = 10\,000$ and $\mathcal{T} = 400$. The integration time is measured in units of the thermal diffusion time.

at an unstable fixed point does apparently not vary. But during the relaxation towards the state shown a monotonic prolongation of this waiting time could be observed. Such a prolongation is indicative of a stable (attracting) heteroclinic cycle. The fact that the cycle length does not tend to infinity is very probably due to finite numerical precision (this effect of the numerics is, *e.g.*, discussed in Ref. [47], Sect. 6.3). One should also note that the cycle length is indeed very large, of the order of 10^4 thermal diffusion times.

For $\mathcal{T} = 400$ (and $\mathcal{R} = 10\,000$) we have calculated the eigenvalues and eigenvectors of the oblique, intermittent rolls. For each of the two states there are two equal, real positive eigenvalues ($= 15.9$); one eigenvalue vanishes (corresponding to the neutral stability with respect to translations perpendicular to the roll axis); all other eigenvalues have negative real parts. One of the unstable eigenvectors is shown in Figure 5; the other one differs from it merely in that it is translated in the direction of the unperturbed rolls. The largest component of the unstable eigenvectors is either the mode $(0, \mp 1, 1)$ (as in the example shown in

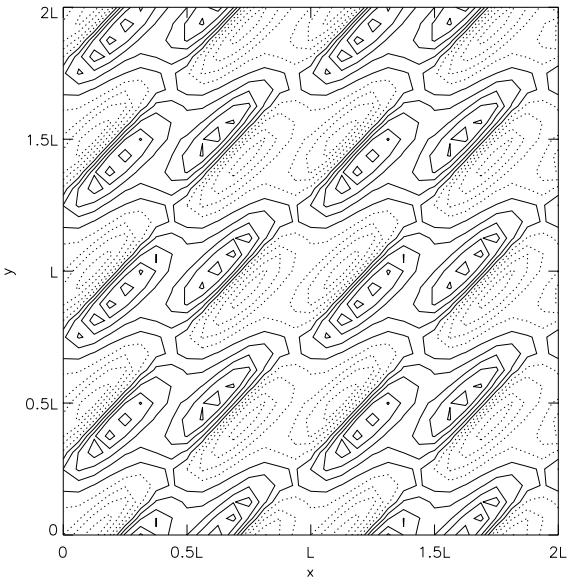

Fig. 5. Unstable eigenvector to one of the intermittent fixed points, calculated for $\mathcal{R} = 10\,000$ and $\mathcal{T} = 400$. Isolines of the vertical velocity component v_z in the horizontal midplane are shown. Solid (dashed) lines refer to positive (negative) values.

Fig. 5, corresponding to rolls parallel to the y axis) or (for the other oblique-roll state) $(\mp 1, 0, 1)$, followed by shear components independent of z (*e.g.* $v_x(0, \mp 1, 0)$ in the example shown in Fig. 5) as well as components with higher mode numbers. The unstable eigenvectors show the same tilt of structures as do the respective unperturbed states; the eigenvector shown in Figure 5, for instance, belongs to the roll solution with rolls rotated clockwise by 45° with respect to the y axis. If a certain percentage disturbance (unstable eigenvector) is superposed to the unperturbed rolls, the resulting structure looks similar to that shown in Figure 11 and is strongly suggestive of the skewed-varicose instability [5].

The overall behavior observed is similar to that in the Busse-Clever-Heikes [8,9] model for Küppers-Lortz unstable rolls. The numerics brings in a lower bound to the distance between the phase-space trajectory and the saddle points. It thus acts as experimental noise would do. With one difference, however: Real noise will in general produce a distribution of recurrence times with some tail characteristic (see Ref. [47], Sect. 8.2). The mean noise level (in conjunction with the properties of the unperturbed heteroclinic cycle) introduces a characteristic time scale, the mean recurrence time, also present in our numerical model. What is missing in the numerical model is a detectable variation of the cycle length, seemingly as a consequence of the special character of the "numerical noise" at the resolution boundary.

But there is yet another, striking effect: In Figure 6 the temporal evolution of the real parts of the modes $(-1, 1, 1)$ and $(1, 1, 1)$ is shown. There are considerable amplitude variations, including occasional sign changes. In view of the practically constant amplitudes in Figure 4 (where the moduli of the modes are shown), these variations must be

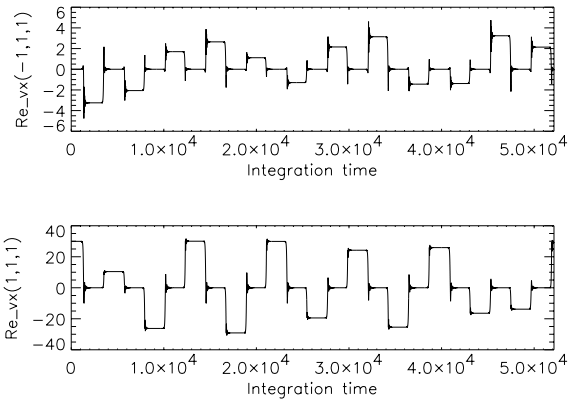

Fig. 6. Time evolution of the real parts of the modes $\tilde{v}_x(-1,1,1)$ and $\tilde{v}_x(1,1,1)$ at $\mathcal{R} = 10\,000$ and $\mathcal{T} = 400$. The integration time is measured in units of the thermal diffusion time.

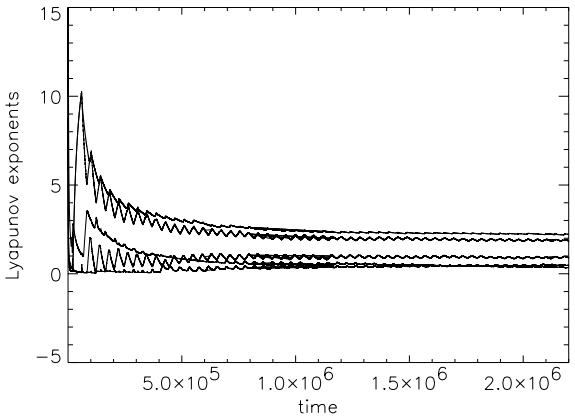

Fig. 7. The 5 largest Lyapunov exponents versus integration time for $\mathcal{R} = 10\,000$ and $\mathcal{T} = 400$. The integration time is measured in units of the thermal diffusion time.

due to phase shifts of the modes, which correspond to horizontal translations of the roll patterns perpendicular to the roll axis.

The time dependence seen in Figure 6 appears irregular. To test for chaos, we have calculated Lyapunov exponents, using an algorithm of Shimada and Nagashima [48]. Figure 7 shows the cumulative values of the 5 largest exponents over the integration time along a system trajectory. As is clearly seen, there are positive exponents. Thus the *calculated* dynamics is chaotic.

According to the above discussion this chaotic behavior requires the presence of noise and would not be observed if the numerical calculations were infinitely precise (since the waiting time at the fixed points would tend to infinity). If roll states transformable into each other by horizontal translations are considered as equivalent, then the attracting state is, seemingly, a heteroclinic cycle, or in other words, the heteroclinic cycle is stable *modulo horizontal translations*. It is important to note, however, that the irregular or chaotic behavior will survive in the limit of vanishing noise or infinite numerical precision. Namely, if a given roll pattern is unstable to a certain perturbation (say, a rotated roll pattern), then, due to the translational symmetry of the original rolls (along the roll axis), these are equally unstable to all perturbations obtained from the first one by horizontal translation. Thus irregular phase shifts or horizontal translations are unavoidable, however small the numerical or experimental noise. This is another mechanism to generate irregularity, in addition to an irregular variation of the cycle length as suggested by Busse, Clever, and Heikes [8,9].

In addition to the calculations for $\mathcal{R} = 10\,000$ described up to now, we have, for the same aspect ratio $L = 2\sqrt{2}$, similarly traced the (time-asymptotic) solutions for $\mathcal{R} = 5\,000$ and $\mathcal{R} = 2\,000$, again starting from the non-rotating case. For $\mathcal{R} = 5\,000$ the scenario is the same as that for $\mathcal{R} = 10\,000$, with onset of heteroclinic behavior now at $\mathcal{T} = 290$. For $\mathcal{R} = 2\,000$ a secondary stable stationary roll solution with rolls lying under -45° or $+45^\circ$ in the box is found between the original rolls and the heteroclinic behavior. These secondary rolls occur at $\mathcal{T} = 250$ and are replaced by heteroclinic behavior at $\mathcal{T} = 350 \ldots 400$.

Furthermore, in order to test for the influence of the aspect ratio, calculations with the larger aspect ratio $L = 4$ and $R = 2\,500$ were made. Without rotation one has then rolls which lie under $\pm 45^\circ$ in the box and whose wavelength is no longer the largest possible one. At $\mathcal{T} = 50$ a transition to a secondary stationary solution of the skewed-varicose type (*cf.* Sect. 5 and Fig. 11) is observed. At $\mathcal{T} = 150$ a Hopf bifurcation leads to a limit cycle showing shearing oscillations of the skewed-varicose pattern. Heteroclinic behavior is observed for $\mathcal{T} \gtrsim 200$. The larger aspect ratio seems to be favorable for an early transition. This is obviously due to the role played by the skewed-varicose instability (see discussion in Sect. 5).

The transition to heteroclinic behavior for fixed Rayleigh number is hysteretic: For $\mathcal{R} = 10\,000$, where for increasing Taylor number the transition takes place at $\mathcal{T} = 360$, following the path backwards to lower Taylor numbers heteroclinic behavior is observed down to $\mathcal{T} \lesssim 250$.

5 Variation of Rayleigh number for fixed Taylor number

We now describe results obtained by varying (increasing) the Rayleigh number for fixed Taylor number:

(i) For $\mathcal{T} = 100$, $\mathcal{T} = 150$, $\mathcal{T} = 175$, $\mathcal{T} = 200$ the primary bifurcation leads to rolls parallel to the y axis. These lose stability to time-periodic states at $\mathcal{R} = 24\,000$, $\mathcal{R} = 26\,000$, $\mathcal{R} = 21\,000$, $\mathcal{R} = 18\,000$. Without rotation a bifurcation from stationary rolls to traveling waves occurs at $\mathcal{R} = 17\,950$ [43]. These traveling waves are of the zigzag (as opposed to the varicose) type. The time-periodic states for $\mathcal{T} = 100$ and $\mathcal{T} = 150$ are also traveling waves of the zigzag type. Then, for $\mathcal{T} = 175$ there is a transition from the stationary rolls to an oscillatory state which is invariant along the roll axis, similar to oscillations found in two-dimensional convection [42]. For $\mathcal{T} = 200$, finally, traveling waves of the varicose type are observed.

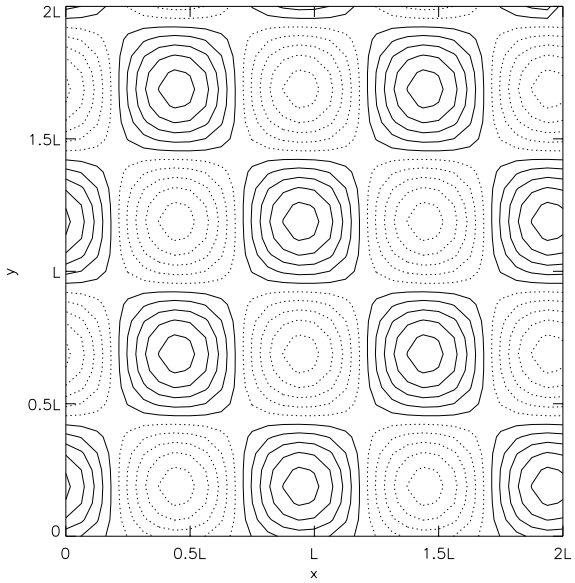

Fig. 8. Isolines of the vertical velocity component v_z in the horizontal midplane for $\mathcal{R} = 1\,100$ and $\mathcal{T} = 250$. Solid (dashed) lines refer to positive (negative) values. Each horizontal periodicity box $(0, L) \times (0, L)$ contains four squares.

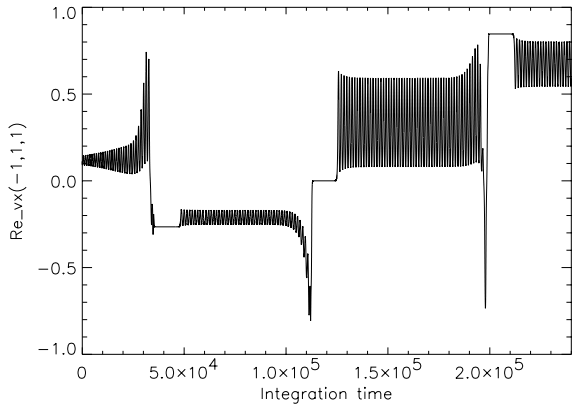

Fig. 9. Time evolution of the real part of the mode $\tilde{v}_x(-1, 1, 1)$ for $\mathcal{R} = 2\,750$ and $\mathcal{T} = 250$. The integration time is measured in units of the thermal diffusion time.

(ii) For $\mathcal{T} = 225$ the primary bifurcation (at $\mathcal{R} = 1\,000$) leads to stationary squares (*cf.* Fig. 8), which (at $\mathcal{R} = 1\,100$) lose stability to stationary rolls lying under $+45^\circ$ or -45° in the periodicity box. At $\mathcal{R} \approx 2\,200$ there is then a bifurcation to a stationary mixed-mode or skewed-varicose-type solution as shown (though for $\mathcal{T} = 300$) in Figure 11, followed, at $\mathcal{R} \approx 2\,500$, by a transition to heteroclinic behavior. At the significantly higher Rayleigh number of $R = 11\,000$ again traveling waves along rolls parallel to a coordinate axis are found.

(iii) For $\mathcal{T} = 250$ the primary bifurcation (at $\mathcal{R} = 1\,100$) still leads to stationary squares (Fig. 8), which (at $\mathcal{R} = 1\,300$) lose stability to stationary rolls lying under $+45^\circ$ or -45° in the periodicity box. At $\mathcal{R} \approx 2\,300$ there is then a bifurcation to a stationary mixed-mode or skewed-varicose-type solution as shown in Figure 11, followed, at

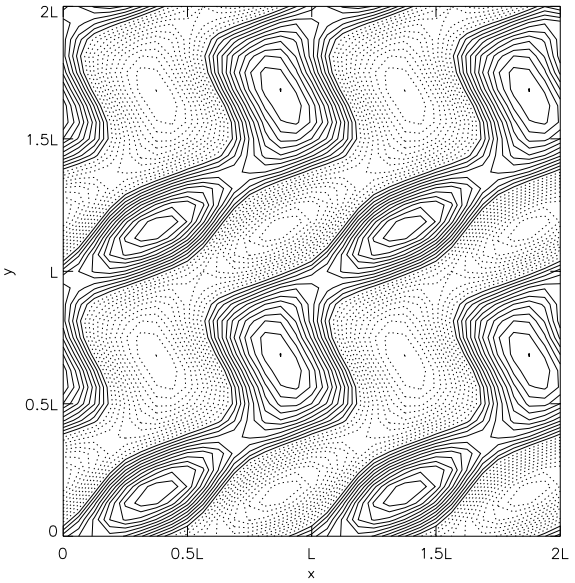

Fig. 10. Isolines of the vertical velocity component v_z in the horizontal midplane for $\mathcal{R} = 2\,750$ and $\mathcal{T} = 250$ (snapshot). Solid (dashed) lines refer to positive (negative) values.

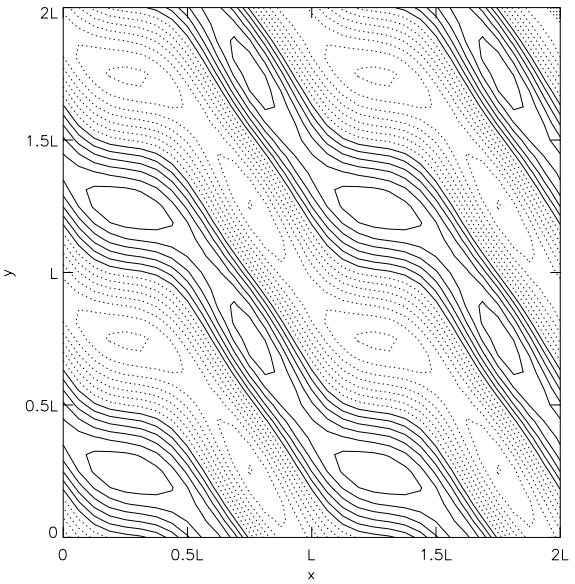

Fig. 11. Isolines of the vertical velocity component v_z in the horizontal midplane for the steady state found at $\mathcal{R} = 2\,400$ and $\mathcal{T} = 300$. Solid (dashed) lines refer to positive (negative) values.

$\mathcal{R} = 2\,700$, by a transition to a heteroclinic behavior showing some interesting details: Again the system switches between -45° and $+45^\circ$ rolls. But the time intervals during which these rolls are visible in pure form are very short compared to oscillatory "transition" phases, as is seen in Figure 9 where the temporal evolution of $\Re\tilde{v}_x(-1, 1, 1)$ is depicted. The oscillations consist of skewed-varicose like deformations of roll-like structures (see Fig. 10). Besides the pure roll pattern (with rolls under $+45^\circ$ or -45°), also a pure square pattern becomes visible during certain short

time intervals. At $\mathcal{R} \approx 3\,000$ this behavior is then replaced by the "normal" heteroclinic behavior as seen in Figure 4.

(iv) For $\mathcal{T} = 300$ the primary bifurcation (at $\mathcal{R} = 1\,100 \ldots 1\,200$) leads to stationary rolls lying under $+45^{\circ}$ or -45° in the periodicity box. A stationary solution of the mixed-mode (skewed-varicose) type appears at $\mathcal{R} = 2\,400$ (see Fig. 11) and heteroclinic behavior is found for $\mathcal{R} = 2\,800$.

(v) For $\mathcal{T} = 2\,500$ and $\mathcal{T} = 3\,000$ (above the critical value for the Küppers-Lortz instability) there is a direct transition from the quiescent ground state to heteroclinic behavior involving four roll states, with rolls rotated by $+26.6^{\circ}$ or -26.6° with respect to the x axis or the y axis (that is, modes with $k_y = \mp 2k_x$ or $k_x = \mp 2k_y$ are excited).

The transition between rolls and squares near the onset of convection is hysteretic: For $\mathcal{T} = 150$, where the primary bifurcation (at $\mathcal{R} = 950$) leads to rolls, simulations starting from *finite-amplitude* squares lead to stationary squares (as shown in Fig. 8). At $\mathcal{R} = 1\,000$ these squares lose stability to stationary rolls lying under $+45^{\circ}$ or -45° in the periodicity box.

Obviously the skewed-varicose instability of rolls [5] is important for the observed heteroclinic behavior. This instability accomplishes a change to larger horizontal wavelengths. It is suppressed if the rolls have the largest possible diameter in a given periodicity box, namely, if there is just one pair of rolls parallel to one of the coordinate axes. Therefore heteroclinic behavior is only found with rolls lying obliquely in the box and having diameters smaller than the maximum one. Increasing the rotation rate decreases the critical horizontal wavelength for the onset of convection (so rolls parallel to a coordinate axis are replaced by rolls lying under $\mp 45^{\circ}$ in box). This corresponds to an increase of the effective aspect ratio. In this way the skewed-varicose mechanism can come into play as a result of an increased rotation rate.

One then wonders whether the onset of heteroclinic behavior is solely due to the increase of the effective aspect ratio with increasing rotation rate. If so, the behavior should also be found in the nonrotating case, provided the aspect ratio is appropriately chosen (sufficiently large). To test this we have traced the nonrotating primary convection rolls towards higher Rayleigh numbers for aspect ratios L of 4, 4.5, and $4\sqrt{2}$. With $L = 2\sqrt{2}$ the rolls were found to become unstable to traveling waves along the roll axis in [43]. For $L = 4$ the primary rolls (whose diameter is $\sqrt{2}$, again just the critical diameter for the onset of convection on an infinite plane) lie under $+45^{\circ}$ or -45° in the box and the situation is similar to that for, say, $\mathcal{T} = 300$ with our standard aspect ratio $L = 2\sqrt{2}$. For $L = 4\sqrt{2}$ one has two pairs of rolls (with the critical diameter) parallel to one of the sides of the box. In all three cases ($L = 4$, $L = 4.5$, and $L = 4\sqrt{2}$) we found the skewed-varicose instability to lead from the primary rolls to stable squares. Figure 12 shows the resulting square pattern for $L = 4$; there is just one square per box, *i.e.*, the horizontal scale has become the largest possible one. The squares are stable up to at least $\mathcal{R} = 9\,000$. For the case of no-slip boundaries and, as in the present study, symmetry of the physical conditions about the horizontal midplane, stable stationary squares of the type shown in Figure 12 were found by Busse and Clever [49]. In summary: Without rotation, the primary rolls lose, depending on the aspect ratio, stability to traveling waves or stationary squares; the horizontal scale is increased when possible (which leads to squares). Skewed-varicose like (final) states and heteroclinic behavior are not found. From this and the results for rotating convection with $L = 4$ described at the end of Section 4 we conclude that, for our Prandtl number of 6.8, a finite amount of rotation is needed to produce heteroclinic behavior.

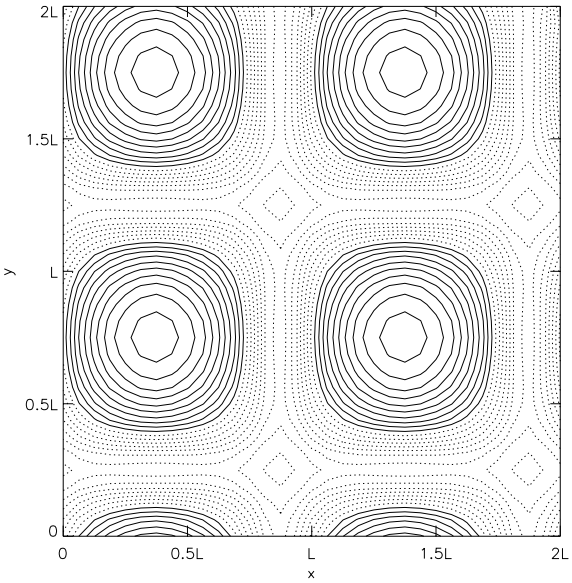

Fig. 12. Isolines of the vertical velocity component v_z in the horizontal midplane for $\mathcal{R} = 2\,000$ and $\mathcal{T} = 0$. Solid (dashed) lines refer to positive (negative) values. The aspect ratio is 4.

6 Conclusion

We have studied rotating Rayleigh-Bénard convection in a plane fluid layer with stress-free top and bottom boundaries and horizontal periodicity on a square lattice. The Prandtl number was fixed to a value of 6.8. The aspect ratio was $2\sqrt{2}$ in most of the calculations and was raised to values of 4, 4.5, and $4\sqrt{2}$ in special additional calculations. Starting from a two-dimensional stable roll solution [43], we included rotation into the problem. The original $[D_2]_{x,z} \times O(2)_y \times SO(2)_t$ symmetry of the roll state is then broken down to a $[D_2]_{x,y,z} \times SO(2)_y \times SO(2)_t$ symmetry.

Keeping the Rayleigh number fixed at values of 10 000, 5 000, or 2 000, we have, with our standard aspect ratio $L = 2\sqrt{2}$, traced the straight-roll solution towards higher Taylor numbers. Heteroclinic behavior sets in at $\mathcal{T} \approx 300$. An additional calculation with the larger aspect ratio $L = 4$ indicated that, obviously due to the role played by the skewed-varicose instability, large aspect ratios are favorable for the transition to heteroclinic behavior.

The heteroclinic dynamics is determined by unstable straight-roll solutions with rolls rotated by $\mp 45^{\circ}$ with respect to the original rolls parallel to one of the coordinate axes. The intermittent, unstable, rotated-roll solutions are still invariant under the symmetry group of the stable (but rotation-influenced) rolls. Their unstable eigenvectors are of the skewed-varicose type. With roll states transformable into each other by horizontal translations considered as equivalent, the attracting state is apparently a (stable) heteroclinic cycle. However, any noise leads to irregular phase shifts or horizontal translations of the rolls, such that, as the calculation of Lyapunov exponents showed, the dynamics becomes chaotic. The irregular horizontal translations of the rolls represent a mechanism to generate irregularity, in addition to an irregular variation of the cycle length as suggested by Busse, Clever, and Heikes [8,9].

We have also studied in detail the transition to heteroclinic behavior by varying the Rayleigh number for fixed Taylor number. The primary bifurcation from the quiescent ground state leads either to stationary rolls or to stationary squares (*cf.* Refs. [50,51]). If squares are selected, there is first a secondary bifurcation to stationary rolls before subsequent bifurcations lead to time-dependent flow, which agrees with results of Riahi [50] for the case of infinite Prandtl number. Of prime importance in the observed bifurcation sequence is the skewed varicose instability, leading from stationary rolls to a stationary mixed-mode solution. This in turn becomes globally unstable to a heteroclinic cycle. There are parameter ranges (with Taylor numbers close to that where at the onset of convection a transition between rolls and squares takes place) where the heteroclinic cycle involves extended phases of skewed varicose like shearing oscillations. Additional calculations with aspect ratios of 4, 4.5, and $4\sqrt{2}$ for the nonrotating case indicated that the heteroclinic behavior is not solely due to the decrease of the effective aspect ratio with increasing rotation rate, but that finite rotation rates are needed. This is different for Prandtl numbers less than one (and, as in the present study, stress-free top and bottom boundaries) [17,18].

A decisive influence of the skewed-varicose instability on the pattern dynamics in rotating convection at small Taylor and Rayleigh numbers was observed in the experiments of Hu, Ecke, and Ahlers [21], albeit for a large aspect ratio, circular geometry, a Prandtl number near one, and no-slip top and bottom boundaries. The skewed-varicose instability appears in the form of pairs of defects in a roll pattern. The defects can travel and thereby cause a pattern rotation. This was observed previously in numerical simulations of rotating convection at large Prandtl numbers by Millán-Rodríguez *et al.* [22,27]. The pattern rotates gradually in the sense of the externally applied rotation. Discrete large jumps as typical of the Küppers-Lortz instability and occuring at higher rotation rates are not observed. Clearly, with periodic boundary conditions and the roll diameter given, the roll orientation can only change by discrete steps. More step-like changes can, for instance, also be expected for rotating convection in square containers, where roll orientation parallel to the sides is preferred. Furthermore, the behavior may vary with variations of the Prandtl number and the aspect ratio. These points need to be explored in future studies.

A.D. wishes to thank T. Passot, P. L. Sulem, M. Zaks, S. Rüdiger, and W. Jansen for helpful discussions. This work was supported in part by Grant No. SE 662/5-1 of the Deutsche Forschungsgemeinschaft (DFG).

References

1. G. Küppers, D. Lortz, J. Fluid Mech. **35**, 609 (1969).
2. G. Küppers, Phys. Lett. A **32**, 7 (1970).
3. R.M. Clever, F.H. Busse, J. Fluid Mech. **94**, 609 (1979).
4. T. Clune, E. Knobloch, Phys. Rev. E **47**, 2536 (1993).
5. F.H. Busse, R.M. Clever, J. Fluid Mech. **91**, 319 (1979).
6. F.H. Busse, in *Hydrodynamic Instabilities and the Transition to Turbulence*, *Vol. 45 of Topics in Applied Physics*, edited by H.L. Swinney, J.P. Gollub (Springer, Berlin, Heidelberg, 1985), pp. 97–133.
7. Y. Ponty, T. Passot, P.L. Sulem, Phys. Fluids **9**, 67 (1997).
8. F.H. Busse, R.M. Clever, in *Recent Developments in Theoretical and Experimental Fluid Mechanics: Compressible and Incompressible Flows*, edited by U. Müller, K.G. Roesner, B. Schmidt (Springer, New York, 1979), pp. 376–385.
9. F.H. Busse, K.E. Heikes, Science **208**, 173 (1980).
10. J. Guckenheimer, P. Holmes, Math. Proc. Cambridge Phil. Soc. **103**, 189 (1988).
11. B. Sandstede, A. Scheel, Nonlinearity **8**, 333 (1995).
12. M. Krupa, J. Nonlin. Sci. **7**, 129 (1997).
13. H.F. Goldstein, E. Knobloch, M. Silber, Phys. Rev. A **46**, 4755 (1992).
14. S. Chandrasekhar, *Hydrodynamic and Hydromagnetic Stability* (Clarendon Press, Oxford, 1961).
15. F.H. Busse, E.W. Bolton, J. Fluid Mech. **146**, 115 (1984).
16. E.W. Bolton, F.H. Busse, J. Fluid Mech. **150**, 487 (1985).
17. F.H. Busse, M. Kropp, M. Zaks, Physica D **61**, 94 (1992).
18. P.C. Matthews, A.M. Rucklidge, N.O. Weiss, M.R.E. Proctor, Phys. Fluids **8**, 1350 (1996).
19. E. Bodenschatz *et al.*, Physica D **61**, 77 (1992).
20. Y. Hu, R.E. Ecke, G. Ahlers, Phys. Rev. Lett. **74**, 5040 (1995).
21. Y. Hu, R.E. Ecke, G. Ahlers, Phys. Rev. E **55**, 6928 (1997).
22. J. Millán-Rodríguez, M. Bestehorn, C. Pérez-García, R. Friedrich, M. Neufeld, Phys. Rev. Lett. **74**, 530 (1995).
23. P. Manneville, *Dissipative Structures and Weak Turbulence* (Academic Press, San Diego, 1990).
24. M.C. Cross, P.C. Hohenberg, Rev. Mod. Phys. **65**, 851 (1993).
25. D. Walgraef, *Spatio-Temporal Pattern Formation* (Springer, New York, 1997).
26. M. Fantz, R. Friedrich, M. Bestehorn, H. Haken, Physica D **61**, 147 (1992).
27. J. Millán-Rodríguez, C. Pérez-García, M. Bestehorn, M. Neufeld, R. Friedrich, Chaos **4**, 369 (1994).
28. Y. Ponty, T. Passot, P.L. Sulem, Phys. Rev. Lett. **79**, 71 (1997).
29. Y. Ponty, T. Passot, P.L. Sulem, Phys. Rev. E **56**, 4162 (1997).

30. K. Julien, S. Legg, J. McWilliams, J. Werne, Phys. Rev. E **53**, R5557 (1996).
31. K. Julien, S. Legg, J. McWilliams, J. Werne, J. Fluid Mech. **322**, 243 (1996).
32. R. Seydel, *Practical Bifurcation and Stability Analysis* (Springer, New York, 1994).
33. G. Müller, A. Ostrogorsky, in *Handbook of Crystal Growth*, edited by D.T.J. Hurle (Elsevier, Amsterdam, 1994), Vol. 2, Chap. 13, pp. 709–819.
34. F. Zhong, R.E. Ecke, V. Steinberg, Phys. Rev. Lett. **67**, 2473 (1991).
35. F. Zhong, R.E. Ecke, V. Steinberg, J. Fluid Mech. **249**, 135 (1993).
36. Y. Liu, R.E. Ecke, Phys. Rev. Lett. **79**, 2257 (1997).
37. L. Ning, R.E. Ecke, Phys. Rev. E **47**, 3326 (1993).
38. Y. Liu, R.E. Ecke, Phys. Rev. Lett. **78**, 4391 (1997).
39. H.F. Goldstein, E. Knobloch, I. Mercader, M. Net, J. Fluid Mech. **248**, 583 (1993).
40. K.M. Bajaj, J. Liu, B. Naberhuis, G. Ahlers, Phys. Rev. Lett. **81**, 806 (1998).
41. E.L. Koschmieder, *Bénard Cells and Taylor Vortices* (Cambridge University Press, Cambridge, England, 1993).
42. E. Zienicke, N. Seehafer, F. Feudel, Phys. Rev. E **57**, 428 (1998).
43. S. Scheel, N. Seehafer, Phys. Rev. E **56**, 5511 (1997).
44. C. Canuto, M.Y. Hussaini, A. Quarteroni, T.A. Zang, *Spectral Methods in Fluid Dynamics* (Springer, Berlin, 1988).
45. W.H. Press, B.P. Flannery, S.A. Teukolsky, W.T. Vetterling, *Numerical Recipes, The Art of Scientific Computing, FORTRAN Version* (Cambridge University Press, Cambridge, England, 1989).
46. E. Hairer, S.P. Nørsett, G. Wanner, *Solving Ordinary Differential Equations I* (Springer, Berlin, 1993).
47. P. Holmes, J.L. Lumley, G. Berkooz, *Turbulence, Coherent Structures, Dynamical Systems, and Symmetry* (Cambridge University Press, Cambridge, England, 1996).
48. I. Shimada, T. Nagashima, Progr. Theor. Phys. **61**, 1605 (1979).
49. F.H. Busse, R.M. Clever, Phys. Rev. Lett. **81**, 341 (1998).
50. D.N. Riahi, Phys. Fluids A **2**, 353 (1989).
51. H.F. Goldstein, E. Knobloch, M. Silber, Phys. Fluids A **2**, 625 (1990).